Author(s): Huang, Yun-Hui & Yamauchi, Hisao & Karppinen, Maarit

Title: Competition between intragranular and intergranular tunneling magnetoresistance in polycrystalline Sr2FeMoO6

Year: 2006

Version: Final published version

Please cite the original version:

Huang, Yun-Hui & Yamauchi, Hisao & Karppinen, Maarit. 2006. Competition between intragranular and intergranular tunneling magnetoresistance in polycrystalline Sr2FeMoO6. Physical Review B. Volume 74, Issue 17. 174418/1-6. ISSN 1550-235X (electronic). DOI: 10.1103/physrevb.74.174418.

Competition between intragranular and intergranular tunneling magnetoresistance in polycrystalline Sr_2FeMoO_6

Yun-Hui Huang,[1,2,*] Hisao Yamauchi,[1] and Maarit Karppinen[1,3]
[1]*Materials and Structures Laboratory, Tokyo Institute of Technology, Yokohama 226-8503, Japan*
[2]*Laboratory of Advanced Materials, Fudan University, Shanghai 200433, China*
[3]*Laboratory of Inorganic and Analytical Chemistry, Helsinki University of Technology, Espoo 02015, Finland*
(Received 22 July 2006; revised manuscript received 3 October 2006; published 17 November 2006)

Polycrystalline Sr_2FeMoO_6 (SFMO) samples with various grain sizes and densities of Fe/Mo disorder defects were synthesized from sol-gel-derived precursors by means of a sample-encapsulation technique. The samples with perfect Fe/Mo ordering exhibited metallic transport behavior and a large magnetoresistance (MR) effect, whereas the samples with a high-disorder density and small grain size showed a metal-insulator transition and lower MR values. It is suggested that a competition between intragranular and intergranular tunneling MR effects exists in the SFMO system. To confirm this competition, homocomposite samples consisting of two or three single-phase SFMO components with different grain sizes were designed. Large enhancement in low-field magnetoresistance (LFMR) was observed in the homocomposites, which could be attributed to the enhanced intergranular effect. It is thus concluded that the intergranular effect is more important to the LFMR than the intragranular effect.

DOI: 10.1103/PhysRevB.74.174418 PACS number(s): 75.47.Gk, 72.25.−b, 72.80.Ng, 75.30.Kz

I. INTRODUCTION

The *B*-site ordered $A_2B'B''O_6$-type double-perovskite oxide, Sr_2FeMoO_6 (SFMO), has been extensively investigated since the discovery of its half-metallic electronic structure and striking tunneling magnetoresistance (TMR) effect. The spin-polarized charge carrier tunneling persists even up to room temperature due to high Curie temperature.[1,2] Previous studies have revealed that the technologically interesting low-field magnetoresistance (LFMR) of SFMO is affected by various material parameters such as misplaced Fe/Mo atoms, antiphase boundaries, size of the grains, impurity phases, etc.[3–14] It is believed that two types of tunneling effects, namely intragranular and intergranular tunneling, exist in SFMO simultaneously. The former refers to the intrinsic two-dimensional defects such as the Fe/Mo disorder defects (DODs), antiphase boundaries (APBs), and some domain boundaries.[2,9,10] The latter is ascribed to grain boundaries (GBs) and even to impurity-phase grain boundaries.[12–14]

A certain density of DODs remains unavoidably on the octahedral *B*-cation sublattice in SFMO after a finite sintering period owing to the slow kinetics of the ordering process.[15] In SFMO, a long-range magnetic interaction between the spins of Fe^{3+} ($S=5/2$) and Mo^{5+} ($S=1/2$) induces the ferromagnetic half-metallic state with a theoretical saturation magnetization (M_s) of $4\mu_B$ per formula unit. With the existence of DODs, the M_s value should be lowered due to the antiferromagnetic interaction between the adjacent Fe ions. Furthermore, the DODs produce a reduction in the electron spin polarization at the Fermi level, and hence affect the TMR properties. García-Hernández *et al.*[3] observed a linear dependence of LFMR with M_s, which was related to the DODs at the Fe and Mo sites. Sarma *et al.*[7] found that the ordered sample exhibited a spectacular low-field MR response. More recently, ^{57}Fe Mössbauer spectroscopy revealed the existence of APBs between regions where the ideal alternating stacking of Fe and Mo atoms starts from the opposite cations.[9] It was also shown that the strong antiferromagnetic (AF) coupling between spins of the APB atoms affects the LFMR property.

In addition to the DODs, the GB effect also plays an important role in the magnetotransport property, especially in the case of LFMR. Yin *et al.*[6] attributed the LFMR to electron spin dependent transfer across GBs for an epitaxial SFMO film grown on a bicrystal boundary. Niebieskikwiat *et al.*[8] found that GB insulating barriers are most important to improve the MR property in SFMO. Enhanced LFMR has been observed in some nanoscaled samples, in which the low coercive field facilitates easy rotation of small magnetic domains.[12–14] Sharma *et al.*[16] found a significantly improved LFMR in a bulk sample and attributed it to grain boundary oxygen loss that was controlled through the sintering process. Therefore, the sample itself and the preparation process are the key points for the MR effect and the corresponding mechanism.

Although the influences of DODs and GBs on the MR characteristics have been investigated extensively, some of the mechanisms still remain ambiguous. This is due to the fact that through conventional sample synthesis techniques it is impossible to independently control the various material parameters that may affect the MR property. In this work, homogeneous ("single-component") SFMO samples with various grain sizes and degrees of Fe/Mo order and also "homocomposite" samples containing two or three different SFMO components were designed for investigating the contributions from DODs and GBs to the MR characteristics. It was revealed that the MR strongly depends on both DODs and GBs. Large enhanced MR was attained in the homocomposites. A competition between intragranular and intergranular tunneling effects is suggested to dominate the TMR behavior in SFMO.

II. EXPERIMENTAL

A wet-chemical method was employed to prepare Sr_2FeMoO_6 samples, as described elsewhere in detail.[17] In

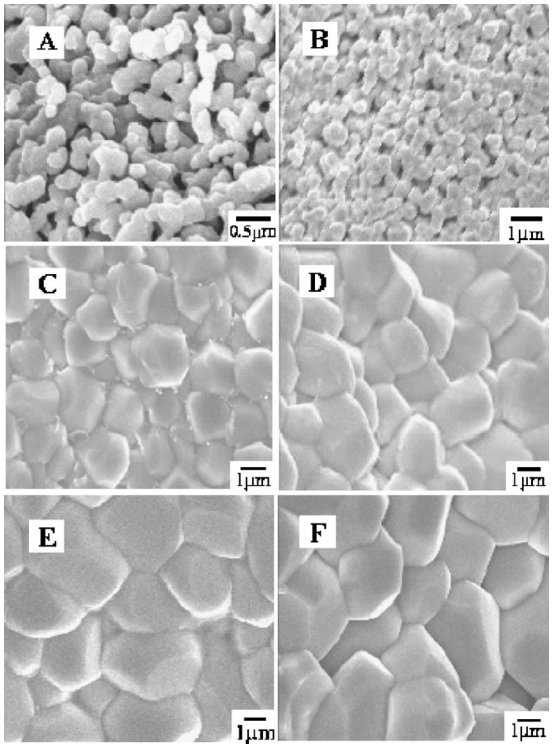

FIG. 1. SEM images for the Sr_2FeMoO_6 samples sintered under different conditions: (a) 900 °C, 24 h; (b) 1000 °C, 50 h; (b) 1150 °C, 4 h; (b) 1150 °C, 24 h; (e) 1150 °C, 50 h; and (f) 1150 °C, 100 h.

brief, stoichiometric amounts of $SrCO_3$, $Fe(NO_3)_3 \cdot 9H_2O$, and $(NH_4)_6Mo_7O_{24} \cdot 4H_2O$ were used as starting chemicals, and ethylenediaminetetraacetic acid (EDTA) as a complexant. The precursor powder was obtained by thermal decomposition of the complex gel, which was then calcined in air at 900 °C for 15 h. Single-phase SFMO samples were obtained by firing the precursor pellet encapsulated in an evacuated fused-quartz ampule containing Fe grains as a getter for excess oxygen[18] at a temperature (T_s) ranging from 900 to 1150 °C for different periods of time (t_s). We refer to the sample sintered at 900 °C for 24 h, 1000 °C for 50 h, 1150 °C for 4, 24, 50, and 100 h by SFMO-A, -B, -C, -D, -E, and -F, respectively.

Homocomposite SFMO samples were fabricated with a two-step route. The above SFMO-F powder (with the largest grains and the highest degree of order) was used as the main component. It was mixed with the precursor powder in various weight ratios, pelletized, encapsulated again into an evacuated ampule together with Fe grains, and finally fired at 950 °C for 8 h. Thus the homocomposite sample consisting of SFMO grains with two different sizes was realized. We denote by x the weight fraction of SFMO-F in the composite.

The phase purity and the lattice parameters were checked by x-ray powder diffraction (XRD). The data were collected at room temperature from $2\theta=20°$ to 100° with a step of 0.02° using a D/max-2000 diffractometer (Rigaku) equipped with a rotating Cu anode. The diffraction profiles were analyzed with a Rietveld refinement program, RIETAN 2000. As a parameter for the density of DODs, we calculated the fraction of misplaced Fe atoms as $w \equiv 1 - g_{Fe}$, where g_{Fe} is the refined occupancy of Fe at its correct site. Hence, for a completely ordered (disordered) sample w is 0 (0.5). Micrographs taken from the samples by a scanning electron microscope (SEM; Hitachi: S4500) were used for the grain size (D) estimation. Magnetization measurements were performed on a superconducting quantum interference device (SQUID; Quantum Design MPMS-XL5). Electrical resistivity was measured using a standard four-probe technique with a commercial apparatus (PPMS; Quantum Design System-Model 6000).

III. RESULTS AND DISCUSSION

A series of SFMO samples with a variety of w and D values was obtained through sample sintering at 900 −1150 °C for different time periods. X-ray diffraction patterns indicate that all the samples are of pure double-perovskite phase. The patterns are well refined in tetragonal space group, $I4/m$. The structural parameters calculated by Rietveld refinement are listed in Table I. The w value decreases with increasing sintering temperature, T_s. As reported in our previous works, sintering at 1150 °C facilitates a low w value due to thermal equilibrium.[15,17] For a sample sintered at 1150 °C, w is about 0.05 for t_s=4 h, 0.03 for 24 h, and as low as 0.02 for 100 h. Figure 1 shows SEM images for SFMO samples A-F. All the samples look highly homogeneous. The sample SFMO-A shows round grains with an average diameter of about 0.1 μm. As T_s increases, the grain size becomes larger and the crystallization more perfect. For SFMO-B, the grains are cubic with $D \approx 0.4$ μm. When T_s =1150 °C, polyhedral grains are achieved, and the grain size increases with t_s. For samples with a fixed t_s, D increases and w decreases with increasing T_s. The variation of D and w in respect to T_s is seen from Table I. In general, a less-ordered sample exhibits a smaller D. For example, D of the sample with w=0.22 is only about 0.1 μm. On the other hand, if the sample is sintered at the same T_s, D increases and w decreases with prolonging t_s.

Figure 2 shows magnetization as a function of applied

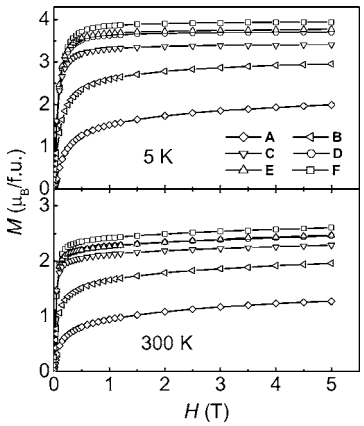

FIG. 2. Magnetization as a function of applied field at 5 and 300 K for the Sr_2FeMoO_6 samples (SFMO A-F) sintered under different conditions.

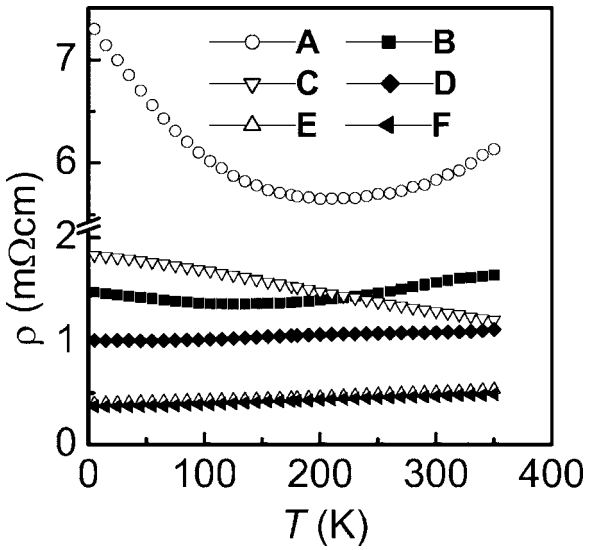

FIG. 3. Temperature dependence of zero-field resistivities for the Sr_2FeMoO_6 samples (SFMO A-F).

field at 5 and 300 K for the SFMO samples. The M_s value is obtained from extrapolation of M versus $1/H$ to $H=0$. As listed in Table I, for 1150 °C-sintered samples M_s at 5 K is $3.48\mu_B$ for $t_s=4$ h, $3.74\mu_B$ for $t_s=24$ h, $3.82\mu_B$ for $t_s=50$ h, and $3.88\mu_B$ for $t_s=100$ h, fitting well the theoretical expectation, $M_s=4(1-2w)\mu_B$. Hence the high experimental M_s values confirm the good cationic ordering in our SFMO samples sintered at 1150 °C. In addition, M_s at 300 K is as large as $2.6\mu_B$ when $t_s \geqslant 24$ h, illustrating a high spin polarization even at room temperature. However, samples SFMO-A and SFMO-B that were sintered at lower temperatures exhibit lower M_s values due to higher DOD densities.

Resistivity at zero field as a function of temperature for the SFMO samples is presented in Fig. 3. The metal-insulator behavior is quite different from sample to sample due to the different w and D values. The sample SFMO-C completely behaves as an insulator, whereas SFMO-E and SFMO-F are metallic. For SFMO-A, SFMO-B, and SFMO-D, an upturn, i.e., a transition from a metallic to an insulatinglike state, appears on the resistivity curve upon cooling. The upturn temperatures of SFMO-A, SFMO-B, and SFMO-D are 210, 126, and 60 K, respectively. Ideally SFMO should exhibit intrinsic metallic state within the measured temperature range (5–350 K) because of the high Curie temperature of above 400 K. Obviously, sintering at a low temperature or at a high temperature for a short time is not enough to eliminate the influence of GBs. The existence of GBs causes the transport properties to depend on thermal scattering carriers, as commonly seen for polycrystalline ceramic samples.[1] We believe that the grain size and connection between grains play important roles in the transport property. Small grains and weak connection lead to a large amount of boundaries and interfaces, and hence a large residual resistance. GBs not only affect the behavior of resistivity in terms of temperature, but also the absolute values of it. If the sample is sintered at 1150 °C for more than 50 h, it exhibits a metallic state, and the absolute resistivity values become very low. The magnitude of resistivity for SFMO-E

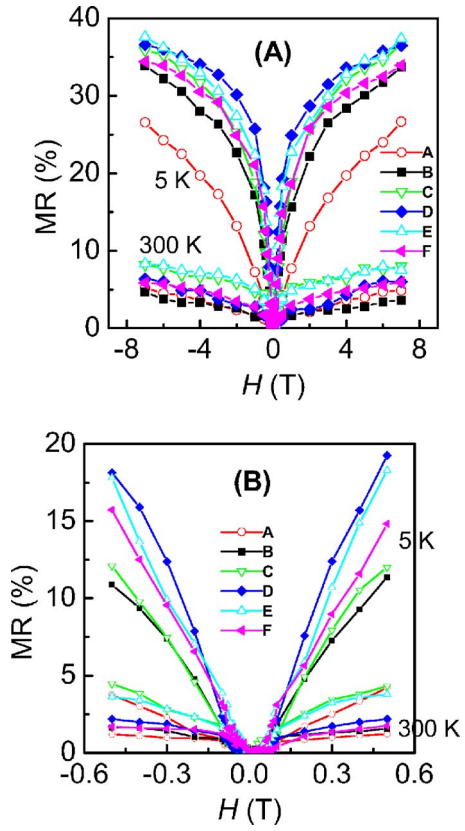

FIG. 4. (Color online) (a) Magnetoresistance ratio (MR) as a function of applied field, and (b) low-field MR at 5 and 300 K for the Sr_2FeMoO_6 samples (SFMO A-F).

and SFMO-F ranges from 0.3 to 0.6 mΩ cm, almost approaching the value typically reported for the single-crystal sample.[20] This demonstrates that our polycrystalline samples sintered at 1150 °C for adequately long periods are dense enough to eliminate the residual resistance from the grain-boundary phase, and thus they exhibit intrinsic transport behaviors.[19] However, SFMO-C behaves as an insulator even though it was also sintered at 1150 °C. This is because t_s is not long enough for tight connection between the grains. It is thus concluded that GBs are the predominant factor to determine the zero-field transport properties.

Figure 4(a) shows the magnetoresistance ratio (MR) for the SFMO samples (A-F) as a function of applied field (H) at 5 and 300 K. The MR ratio is defined as $MR \equiv (\rho_0-\rho_H)/\rho_H$, where ρ_0 and ρ_H are resistivities at zero field and an applied field, respectively. Two regimes are observed on the MR curves. MR increases with a steep slope when the field is lower than 1 T (LFMR region), but more slowly with a further increase in field. Figure 4(b) shows the MR in the low field region for the SFMO samples. Samples D-F exhibit more sensitive MR at low applied fields than SFMO-C at 5 K; however, the LFMR at 300 K of SFMO-C is comparable to that of SFMO-E. SFMO-A and SFMO-B, which were sintered at lower temperatures, exhibit low TMR values in the entire H range measured.

The magnetotransport property of SFMO strongly depends on the density of DODs, APBs, grain size, etc. The three samples, SFMO-D, SFMO-E, and SFMO-F, present a

TABLE I. Structural parameters, goodness-of fit parameters (R_{WP} and R_P) and occupancy of Fe atoms at their right site (g_{Fe}) deduced from the Rietveld refinement of XRD data at room temperature. Fraction of misplaced Fe or Mo atoms (w) calculated from g_{Fe}, average grain size (D), saturation magnetization (M_s), and magnetoresistance ratio (MR) at 5 and 300 K are also given (the M_s value was obtained from extrapolation of M vs $1/H$ to $H=0$).

Sample	SFMO-A	SFMO-B	SFMO-C	SFMO-D	SFMO-E	SFMO-F
Sintering condition	900 °C	1000 °C	1150 °C	1150 °C	1150 °C	1150 °C
	24 h	50 h	4 h	24 h	50 h	100 h
a (Å)	5.5801(1)	5.5768(1)	5.5754(1)	5.5754(1)	5.5754(1)	5.5754(1)
c (Å)	7.8836(3)	7.9006(2)	7.9049(1)	7.9049(2)	7.9057(1)	7.9052(1)
V (Å^3)	245.48(1)	245.72(1)	245.72(1)	245.73(1)	245.75(1)	245.74(1)
R_{wp} (%)	11.12	12.26	11.71	12.14	9.96	10.52
R_p (%)	7.82	9.37	8.75	9.26	7.65	7.75
Goodness of fit	2.70	2.86	2.65	2.84	2.72	2.54
g_{Fe}	0.8061	0.8754	0.9567	0.9707	0.9717	0.9760
w	0.194	0.125	0.043	0.029	0.028	0.024
D (μm)	0.1	0.3	1.9	2.4	3.3	3.8
M_s(μ_B/f.u.), 5 K	2.24	3.16	3.48	3.74	3.82	3.88
M_s(μ_B/f.u.), 300 K	1.43	2.13	2.37	2.62	2.66	2.67

remarkably high degree of Fe/Mo ordering. As seen from Table I, SFMO-F sintered for a long period at 1150 °C is almost perfect in cationic ordering, the value of w being as low as 0.024. No obvious difference in MR effect is observed between SFMO-D and SFMO-E though a small difference in w exists between them. However, SFMO-F with the lowest DODs shows a slightly lower MR compared to SFMO-D and SFMO-E. SFMO-A and SFMO-B exhibit much lower MR values. We believe that both DODs and GBs play important roles in the MR characteristics. In other words, intragranular and intergranular tunneling effects competitively coexist in the SFMO system. Intragranular property arises from the suppression of spin fluctuations under the application of almost saturated magnetic field, predominating the intrinsic high-field MR (HFMR) behaviors. That is why the HFMR magnitudes for SFMO-A and SFMO-B are much lower than for other samples. The sample with lower DODs shows higher HFMR. As for the LFMR, it mainly correlates with the factors related with the GBs, e.g., the grain size, the connection between grains, and the crystallinity of the intragranular material. The disordered spins at the GBs can easily array along the direction of an external field (even at low applied fields), yielding the LFMR effect. The ideal sample with optimal LFMR should have small grains with high saturation magnetization and high spin polarization. For SFMO-A and SFMO-B, grain boundary effects are remarkable due to the small grain size and the low density caused by low sintering temperature, whereas the density of DODs is high and accordingly the M_s values are low. The competition between intra- and intergranular tunneling makes the MR effect weak. However, HFMR and LFMR are both significant for samples D-F with low DODs. Therefore, high cationic ordering is the precondition for achieving remarkable TMR effects.

Both D and w strongly depend on sintering conditions. For example, sintering at a low temperature leads to a small grain size but high density of DODs. It is difficult to change D at a fixed w, or to change w at a fixed D. From the view of sample synthesis technique, it is almost impossible to separate intragranular TMR from intergranular TMR, and vice versa. To gain further insight into the intergranular tunneling effect, we should compare the MR characteristics of several samples with different GB densities but of almost the same w value. Thus homocomposite samples were designed to obtain artificial boundaries, in which perfectly ordered SFMO was used as the main component and less-ordered SFMO as the second or even the third component.

Figure 5 shows SEM images for the typical two-component homocomposite samples with $x=0.9$, 0.8, and 0.5, and also for the sample SFMO-811. Here, SFMO-811 is a composite consisting of three kinds of SFMO components, i.e., 80 wt % SFMO-F; 10 wt % 1000 °C-calcined SFMO, and 10 wt % 900 °C-calcined SFMO. It can be seen clearly that the large grains are surrounded by the smaller ones. The

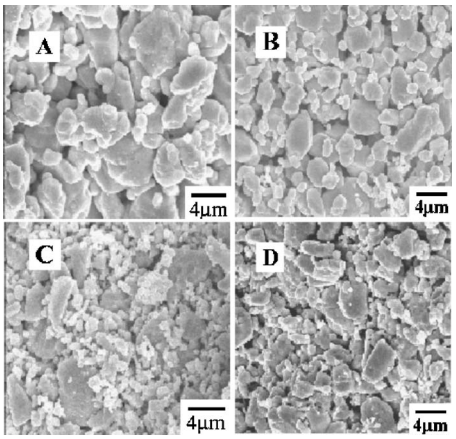

FIG. 5. SEM images for the Sr_2FeMoO_6 homocomposites: (a) $x=0.9$; (b) $x=0.8$; (c) $x=0.5$; and (d) SFMO-811.

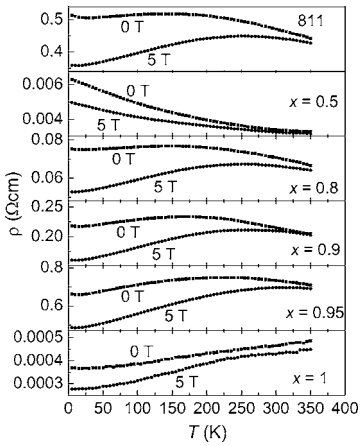

FIG. 6. Temperature dependence of resistivity (ρ) at 0 and 5 T for the homocomposites with $x=1$, 0.95, 0.9, 0.8, and 0.5.

small grains are filled into the interspace of the large grains. The average grain size D of the main component is $\sim 3.8\ \mu$m. For the second SFMO phase in the two-component composites, D is $\sim 1.0\ \mu$m. In SFMO-811, the values of D for the three components are 3.8, 1.5, and 0.5 μm, respectively.

Figure 6 presents the temperature dependence of resistivity at 0 and 5 T for the two-component homocomposites with $x=1$, 0.95, 0.9, 0.8, and 0.5. For $x=1$, the resistivity shows a slight increase with temperature, and the value is around 0.4 mΩ cm, indicative of a metallic state. With incorporation of small grains, the transport behavior changes remarkably. As x decreases, a metal-insulatorlike transition peak appears. When $x=0.5$, the sample exhibits insulatorlike behavior over the entire measured temperature range. The values of the resistivities are quite different from sample to sample, indicating that the resistivities of the composites are dominated by the carrier scattering at the GBs, as commonly observed in polycrystalline ceramic samples.[21] The spin-dependent scattering is not due to the bulk phenomenon arising from the thermal fluctuation of spins but occurs at the GBs or at the magnetic domain boundaries. Due to a strong Hund's interaction, spin disorder around GBs serves as a strong scattering center for the highly spin-polarized conduction electrons and results in a high zero-field electrical resistance.[22]

In Fig. 7(a), plots of MR versus H are shown for the homocomposites with various x values. All samples exhibit two distinguishable regions in the field dependence of MR. MR increases rapidly for $H \leqslant 0.5$ T but rather moderately for $H > 0.5$ T with increasing H. Compared with the $x=1$ sample, the composites with $x=0.7-0.95$ achieve a clear enhancement in MR at both 5 and 300 K. As demonstrated in our previous paper,[23] the MR value of the homocomposites is proportional to the square of the relative magnetization (M/M_S), which reinforces the tunneling effect in the magnetotransport process. Among the two-component composites, the $x=0.8$ sample exhibits the maximal HFMR. The low-field MR is presented in Fig. 7(b). We can clearly see that the $x=0.8$ and $x=0.9$ samples almost gain an identical LFMR enhancement, and that SFMO-811 shows the largest LFMR.

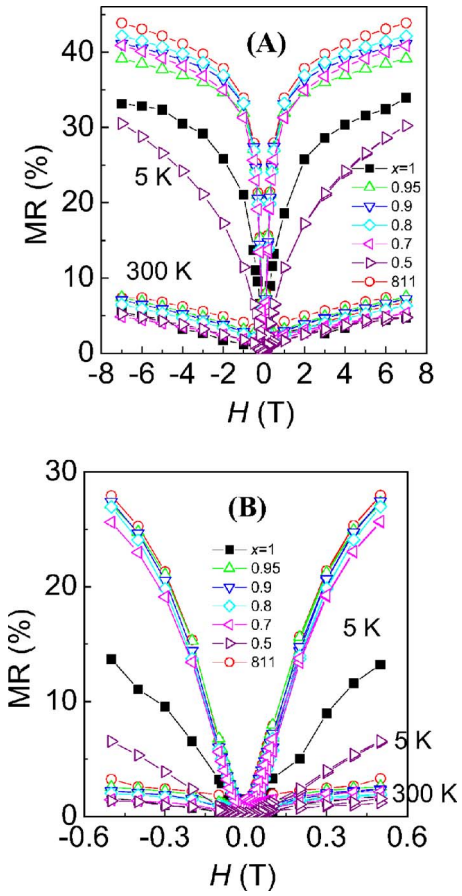

FIG. 7. (Color online) (a) Magnetoresistance ratio (MR) as a function of applied field, and (b) low-field MR at 5 and 300 K for the homocomposites with $x=1$, 0.95, 0.9, 0.8, and 0.5.

For the $x=0.8$ and SFMO-811 samples, the shapes of the resistivity versus temperature curves are similar but the magnitude of resistivity for the latter is about seven times larger than that for the former (Fig. 6). Both HFMR and LFMR ratios of the latter are obviously higher than those of the former (Fig. 7). Since the two samples have the same concentration of the main component, the contribution to TMR from DODs should be comparable. It is thus concluded that the GB effects (including interspace and connection between grains) strongly affect the electronic transport and TMR properties.

The MR enhancement can be further explained by spin disorder at GBs. As shown in the magnetic hysteretic loop (Fig. 8), the coercivity (H_c) is only 38 Oe (4 Oe) at 5 K (300 K) for SFMO-F, being much lower than those reported for other polycrystalline and thin-film SFMO samples.[1,7] For the two-component homocomposite samples, H_c increases as x decreases. The reduction in H_c can be attributed to the disordered spins at GBs that dilute the ferromagnetism. The presence of disordered spins is indicative of a short-range magnetic order. For the fully ordered double perovskite Sr_2FeMoO_6, alternating Fe^{3+} ($3d^5$, $S=5/2$) and Mo^{5+} ($4d^1$, $S=1/2$) ions are ferrimagnetically coupled. If DODs exist, antiferromagnetic Fe-O-Fe and paramagnetic Mo-O-Mo patches will be buried into the ferromagnetic Fe-O-Mo matrices. For the composites, the fraction of small grains in-

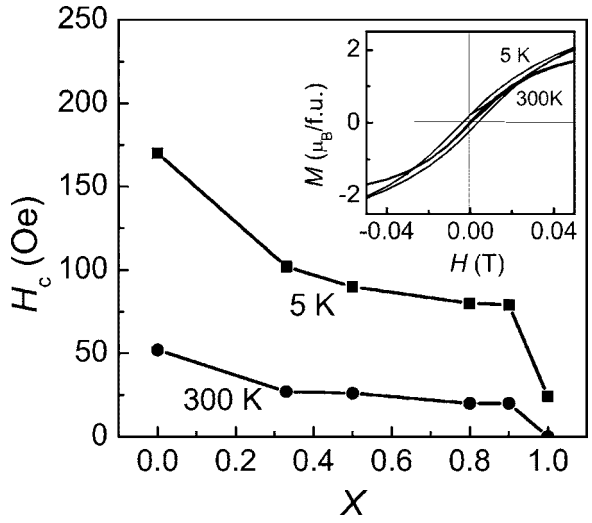

FIG. 8. Coercivity vs x for the homocomposites. The inset shows isothermal magnetization loop of sample SFMO-F measured at 5 and 300 K. Saturation moment was $3.88\mu_B$/f.u. at 5 K and $2.67\mu_B$/f.u. at 300 K. Coercivity was 38 Oe at 5 K and 4 Oe at 300 K.

creases with decreasing x, and thus the effects of GBs and DODs both become more remarkable. The spins in the GBs and DODs depend strongly on the temperature and the magnitude of the applied magnetic field. With a moderate external magnetic field, the spins can be easily aligned along the field direction. The suppression of disordered spins makes an additional contribution to the significant LFMR in the homocomposite samples.

IV. CONCLUSIONS

A series of Sr_2FeMoO_6 samples with different values for D (=grain size) and w (fraction of misplaced Fe or Mo atoms), and also two-component and three-component homocomposites were designed to investigate intragranular and intergranular tunneling MR effects in Sr_2FeMoO_6. The MR values of various samples were compared. Lower w values give rise to higher MR values, and vice versa. On the other hand, the resistivity also strongly depends on D and w. Perfectly ordered samples exhibit a metallic transport behavior, whereas the samples with large w and small D showed a metal-insulator transition or even an insulating behavior. The homocomposite samples with a large amount of GBs show a remarkably enhanced low-field MR. Therefore, we suggest a coexistence of intra- and intergranular tunneling MR effects in Sr_2FeMoO_6. The competition between the two kinds of effects determines the magnetoresistance and the transport properties.

ACKNOWLEDGMENTS

This work was supported by a Grant-in-Aid for Scientific Research (No. 15206002) from the Japan Society for the Promotion of Science (JSPS). Y.H.H. acknowledges additional support from JSPS and the National Science Foundation of China (Grant No. 60371011).

*Electronic address: huangyh@mail.utexas.edu

[1] K.-I. Kobayashi, T. Kimura, H. Sawada, K. Terakura, and Y. Tokura, Nature **395**, 677 (1998).
[2] T. H. Kim, M. Uehara, S.-W. Cheong, and S. Lee, Appl. Phys. Lett. **74**, 1737 (1999).
[3] M. García-Hernández, J. L. Martínez, M. J. Martínez-Lope, M. T. Casais, and J. A. Alonso, Phys. Rev. Lett. **86**, 2443 (2001).
[4] A. S. Ogale, S. B. Ogale, R. Ramesh, and T. Venkatesan, Appl. Phys. Lett. **75**, 537 (1999).
[5] H. Q. Yin, J.-S. Zhou, J.-P. Zhou, R. Dass, J. T. McDevitt, and J. B. Goodenough, Appl. Phys. Lett. **75**, 2812 (1999).
[6] H. Q. Yin, J.-S. Zhou, R. Dass, J.-P. Zhou, J. T. McDevitt, and J. B. Goodenough, J. Appl. Phys. **87**, 6761 (2000).
[7] D. D. Sarma, E. V. Sampathkumaran, S. Ray, R. Nagarajan, S. Majumdar, A. Kumar, G. Galini, and T. N. Guru Row, Solid State Commun. **114**, 465 (2000).
[8] D. Niebieskikwiat, F. Prado, A. Caneiro, and R. D. Sánchez, Phys. Rev. B **70**, 132412 (2004).
[9] J. Lindén, M. Karppinen, T. Shimada, Y. Yasukawa, and H. Yamauchi, Phys. Rev. B **68**, 174415 (2003).
[10] T. T. Fang, Phys. Rev. B **71**, 064401 (2005).
[11] J. Navarro, Ll. Balcells, F. Sandiumenge, M. Bibes, A. Roig, B. Martínez, and J. Fontcuberta, J. Phys.: Condens. Matter **13**, 8481 (2001).
[12] C. L. Yuan, S. G. Wang, W. H. Song, T. Yu, J. M. Dai, S. L. Ye, and Y. P. Sun, Appl. Phys. Lett. **75**, 3853 (1999).
[13] H. Han, B. J. Han, J. S. Park, B. W. Lee, S. J. Kim, and C. S. Kim, J. Appl. Phys. **89**, 7678 (2001).
[14] W. H. Song, J. M. Dai, S. L. Ye, K. Y. Wang, J. J. Du, and Y. P. Sun, J. Appl. Phys. **89**, 7687 (2001).
[15] T. Shimada, J. Nakamura, T. Motohashi, H. Yamauchi, and M. Karppinen, Chem. Mater. **15**, 4494 (2003).
[16] A. Sharma, A. Berenov, J. Rager, W. Branford, Y. Bugoslavsky, L. F. Cohen, and J. L. MacManus-Driscoll, Appl. Phys. Lett. **83**, 2384 (2003).
[17] Y. H. Huang, J. Lindén, H. Yamauchi, and M. Karppinen, Chem. Mater. **16**, 4337 (2004).
[18] T. Yamamoto, J. Liimatainen, J. Lindén, M. Karppinen, and H. Yamauchi, J. Mater. Chem. **10**, 2342 (2000).
[19] Y. H. Huang, M. Karppinen, H. Yamauchi, and J. B. Goodenough, Phys. Rev. B **73**, 104408 (2006).
[20] Y. Tomioka, T. Okuda, Y. Okimoto, R. Kumai, K.-I. Kobayashi, and Y. Tokura, Phys. Rev. B **61**, 422 (2000).
[21] M. M. Savosta, V. N. Krivoruchko, I. A. Danielenko, V. Y. Tarenkov, T. E. Konstantinova, A. V. Borodin, and V. N. Varyukhin, Phys. Rev. B **69**, 024413 (2004).
[22] Ll. Balcells, J. Fontcuberta, B. Martínez, and X. Obradors, Phys. Rev. B **58**, R14697 (1998).
[23] Y. H. Huang, J. Lindén, H. Yamauchi, and M. Karppinen, Appl. Phys. Lett. **86**, 072510 (2005).